3.2. Control Design

A design of the above mentioned digital controller is based on computer modeling and frequency-domain (small-signal) and time-domain (large-signal) simulation analyses of the PMSM drive system. Two different control methods for each, current and speed control of the VSI fed PMSM drive system, are analyzed in this chapter. The difference between the two current control methods is related to the existence of the motor back emf elimination in the decoupling circuit. The discussed speed control methods are:

- commonly used control with saturated (open) speed loop and closed current loop control with static PI regulators, designed to respond to the worst case operating conditions, and

- an adaptive controller design, interesting especially for the active load applications, with closed (non-saturated) outer (speed) loop and inner (current) loops, based on the estimation of the load torque slope. The realization of the latter will be discussed in detail.

In principle, a digital feedback current control in d-q space is based on the generation of d and q components of the phase switching duty-cycle signals according to the difference between the current reference and current feedback signals, Figure 15 [57]. The current feedback signals are measured on the PMSM terminals, then filtered, digitally normalized and transformed to d-q coordinates. Characteristic digital effects are considered through the approximation of A/D and D/A sampling and zero-order-hold delays in addition to the delay due to the VSI switching. The current reference signal can be either derived from a reference torque profile, which can be independently defined (torque control without the speed loop), or it can be generated from the output of the speed controller (control with closed speed loop) [52, 57]. In both cases, reference d- and q-axis currents can be modified through the flux-weakening control algorithm for the over-rated speed extensions [63-71], as it is the case in this application. The d-q duty cycle signals from the controller output are transformed to the two-phase stationary (α–β) coordinates and are used as reference signals for the PWM modulator to provide the switching impulses to VSI gate drivers, according to a chosen modulation scheme [76, 78]. A resulting line-to-line voltage on the AC output of the VSI produces the PMSM stator currents, which normalized d-q components follow their d-q references [20, 50, 53, 60].

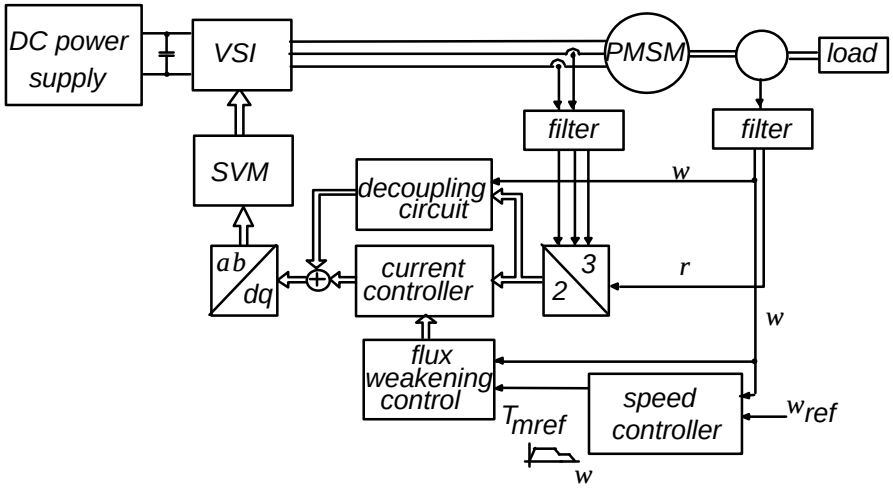

a) Controller principle diagram

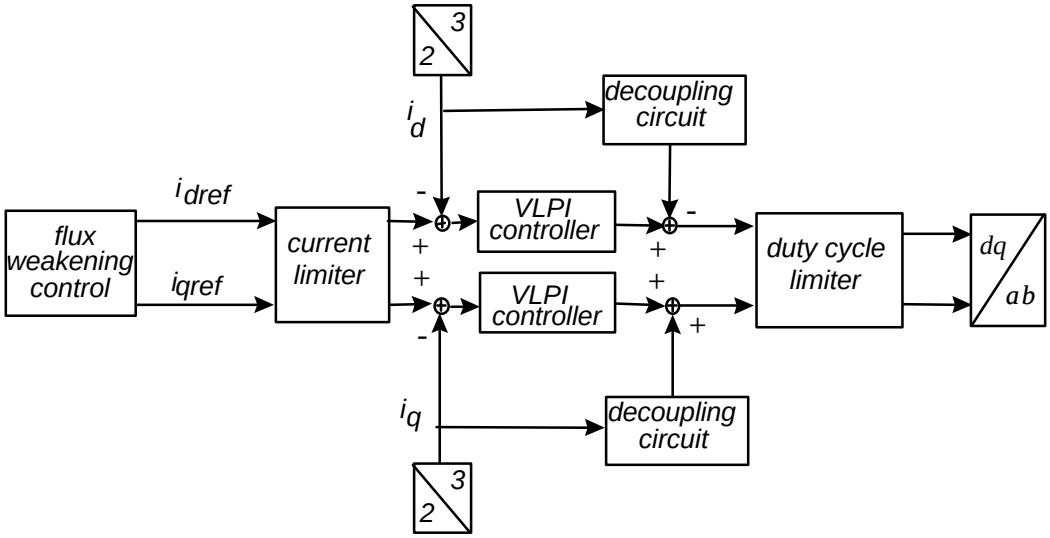

b) A closer look to the current controller

Figure 15. Two stage cascade controller block diagram

The current controller includes two closed current loops in d- and q-axis with variable limit PI regulators (VLPI), voltage and current limiters and a decoupling circuit. The VLPI regulators are PI regulators with implemented integrator reset loops, which close only when the regulator outputs are saturated [79, 80]. A small-signal design of the current regulator PI gains is based on the linearization of the model at several operating points, under artificially provided steady-state conditions. The steady-state conditions, which are never reached in reality during the start-up process (except at zero and final speed), are simulated by artificially adding a constant value to the load torque profile, equal to the motor-load torque difference, i.e. accelerating torque at a particular operating point, Eq. (12). In this way, the system small-signal dynamics and working conditions, regarding the values of electrical variables, are not changed. The d- and q-axis current references are generated by the direct field oriented (DFO) control with various flux-weakening schemes, which will be discussed in Section 3.2.3.

The speed loop controller design is based on control signals of the PMSM rotor position and speed, obtained from a digital resolver, mounted on the PMSM rotor shaft. The resolver transfer function, is approximated as a first order low-pass filter [57]. A generated speed control signal is used as a feedback signal for the speed closed loop control and the decoupling circuit, while the position signal is used as the phase angle reference for the d-q transformation of current feedback signals. A destabilizing effect of the active load is emphasized. Suggested stabilization methods of the speed loop-gain and closed loop transfer functions with an improved “intelligent” controller are explained in detail in Section 3.2.1.

Space vector modulation (SVM) is the chosen technique for modulating the inverter switching signals, because it has a higher phase voltage limit than the sinusoidal PWM scheme, due to injected third harmonic [78]. Analyses of various SVM schemes is given in [25, 59, 72, 76 and 77] and they exceed the scope of this work. Assuming that the switching period used is much smaller than the other motor drive time constants (by at least 5 to 10 times), only the facts about the phase duty cycle limits and the sampling delay effects will be used for the control design, and the whole modulator-VSI system will be represented by the VSI and modulator d-q average models, Figures 2 and 7, respectively.

A controller design procedure is divided in two steps: small-signal control design in the frequency domain and large-signal control design in the time domain.

The small-signal (frequency-domain) design considers the system small-signal behavior with the stress on the stability and step response issues. The scope of the analysis is concentrated on the analysis of characteristic transfer functions of the linearized state-space system model. The classical control theory suggests that the stability issues of a minimum phase system is conveniently analyzed through Bode plots, while Nyquist and/or root-locus diagrams should be used for the stability analysis of systems with right-half-plane poles in its transfer functions (non-minimum phase systems) [57], since their stability issues are not easily observable on Bode plots. It will be shown here that Bode and Nyquist methods have the one-to-one correspondence for frequency-wise single-sided or symmetrical systems, and that even non-minimum phase systems can be analyzed through Bode plots using relatively conservative stability criteria.

The large-signal (time-domain) design considers the implementation of highly non-linear elements, such as signal limiters, flux-weakening control schemes and reference torque or speed profiles, in the controller, with essential parameters (PI gains) obtained from the frequency domain (small-signal) analysis. The stress of the design is on the system large-signal behavior. A mixed level system model containing both three-phase and d-q average module models is used for the purpose of this design. A detailed design of system elements (VSI driver circuits, detailed motor design, protection circuits, filters, etc.) is beyond the scope of this work.

3.2.1. Small-Signal Design

The procedure of the small-signal design will follow a natural constructive path: from the analysis of the features of the considered (non-regulated) system to the loop-by-loop development and design of the control circuits. The controller small-signal design should satisfy the Bode analysis criteria at several critical operating points. These criteria are:

- at a cross-over frequency, ω_c (where the loop-gain magnitude, $|L(s)|_{dB}$, is 0dB), the phase margin, *pm* (calculated as $pm = 180^o + a$, where α is the phase of the loop-gain transfer function at ω_c), has to be large enough to assure the system stability under different operating conditions. A conservative approach is that the phase margin of $pm = 45^o$, assumed to be satisfying regarding the system robustness, should be respected whenever the gain is above -6 dB;

- a gain margin, gm (calculated as gm = 0dB - $|L(s)|_{dB}$) of minimum 6 dB must be assured whenever the phase α is within the phase margin boundaries around the odd multiples of 180^o.

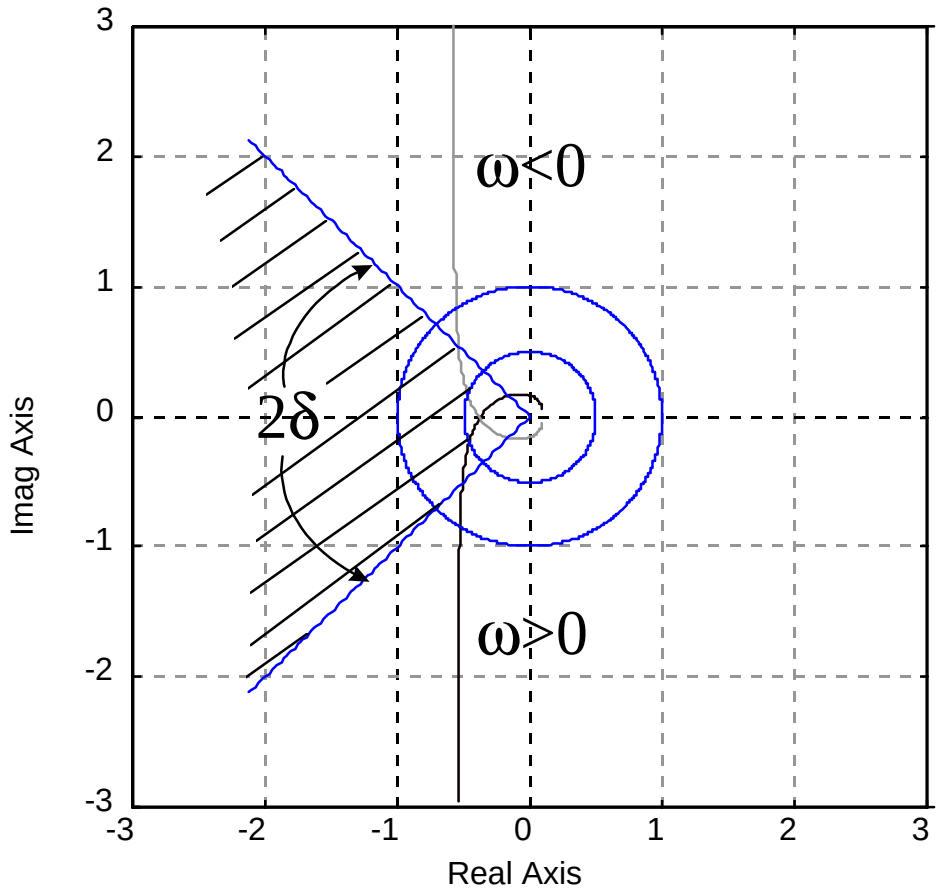

δ - phase margin

Figure 16. Forbidden zones interpreted with Nyquist diagram

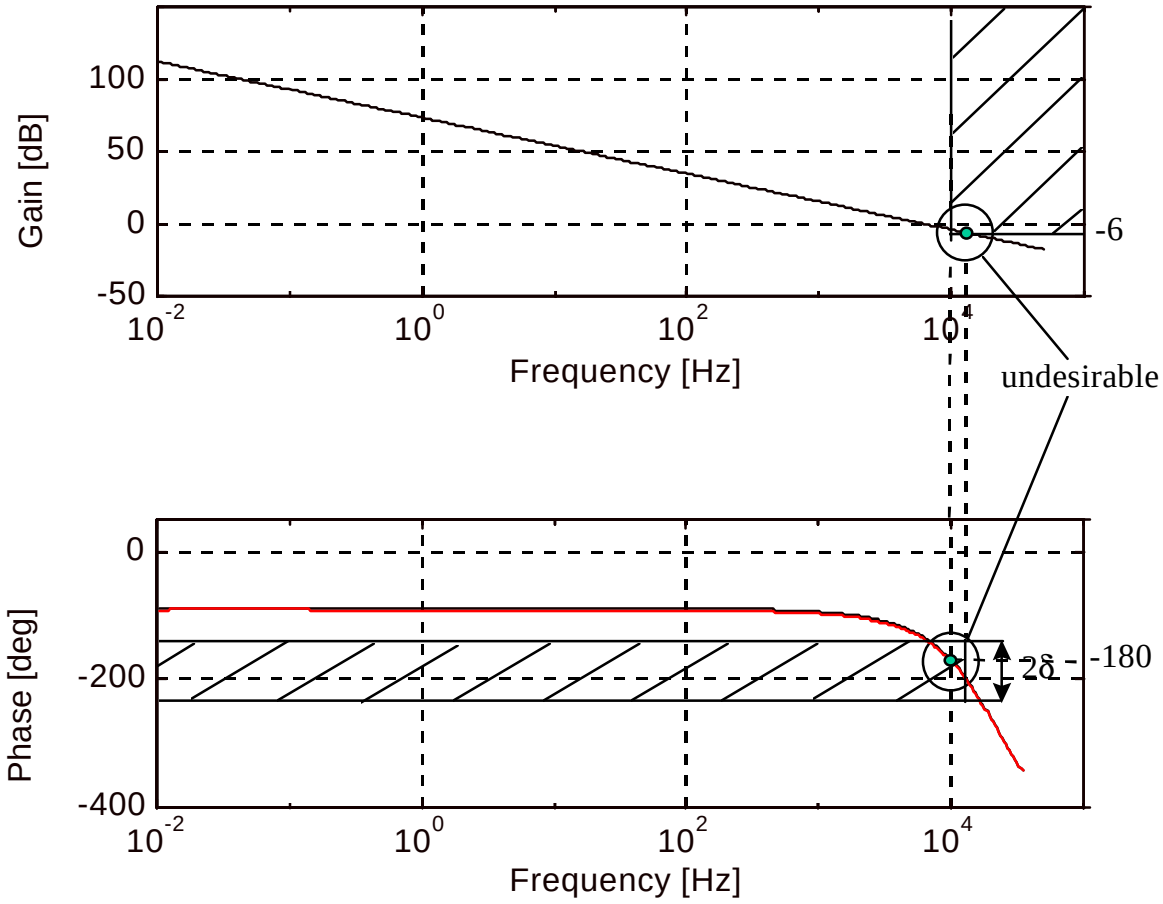

δ - phase margin

Figure 17. Forbidden zones interpreted with Bode plots

These conservative criteria establish a forbidden zone around the point (-1, 0) on the Nyquist plot, i.e. forbid its encirclement, Figure 16. Additionally, it eliminates the local (open loop) instability issues of the system [57]. This forbidden zone on the Nyquist plot maps into two "moving" zones on Bode plots, dependent on the system transfer function gain and phase characteristics, Figure 17. It should be noticed that they are not observable before the system transfer function is plotted out. Then, the phase forbidden zone is established from the gain information and vice-versa. If any of the two (gain and phase) system loop-gain transfer function plots passes through the corresponding forbidden zone, the established stability criteria are violated and the design should be corrected. Although the zones move with a new design, and the gain and phase corrections progress simultaneously, it is pretty straightforward to find a direction for the design changes. The author's opinion is that the Bode plot analysis is the preferred method for a minimum-phase system control design, and, in order to provide the most comprehensive results, it is chosen to be the analysis method in this work. The assumption is that the signal frequency always has a positive sign, or that the system transfer function characteristics are symmetrical regarding the frequency directions, since it is the main restriction of the Bode plot method [57]. Because the operating frequency is directly proportional to the speed of the observed PMSM drive system, the motor neither enters the generative mode in this application, nor changes rotating direction, and there is no evident source of the asymmetrical opposite-frequency harmonic signals, this assumption can be accepted as correct.

3.2.1.1 Plant Description

The first step of the small-signal design is to analyze the small-signal behavior of the linearized, uncontrolled VSI-fed motor drive model in open loop at several operating points and to define the critical ones. The criteria for the critical operating points are:

1) large acceleration slopes of the system, and

2) sampling delay effects on the system transfer functions.

The influence of sampling and zero-order-hold time delays, as well as measurement filters on motor drive transfer functions is considered later in the controller design procedure. The small signal model of the PMSM is derived from its d-q state-space mathematical model, Eq. (12). Every state-space variable in Eq. (12), also shown on the simulation model, Figure 4, can be

expressed as $x = X + \tilde{x}$, where x represents a state-space variable and X and $\tilde{x}$ are its steady state value (at a considered operating point), and small-signal perturbation, respectively. After its implementation in Eq. (12) and after cancellation of the steady state parts, the PMSM d-q small-signal model is:

$$\begin{aligned}
\tilde{v}_d &= R\tilde{i}_d + L_d\frac{d\tilde{i}_d}{dt} - pL_q\Omega\tilde{i}_q - pLI_q\tilde{w} - pL_q\tilde{w}\tilde{i}_q \\
\tilde{v}_q &= R\tilde{i}_q + L_q\frac{d\tilde{i}_q}{dt} + pL_d\Omega\tilde{i}_d + pL_dI_d\tilde{w} + pL_d\tilde{w}\tilde{i}_d + k_t\tilde{w} \\
\tilde{t}_m - \tilde{t}_{load} &= J\frac{d\tilde{w}}{dt} \\
\tilde{t}_m &= \frac{3}{2}((k_t + p(L_d - L_q)I_d)\tilde{i}_q + p(L_d - L_q)I_q\tilde{i}_d + p(L_d - L_q)\tilde{i}_q\tilde{i}_d) \\
\tilde{t}_{load} &= k_{load}\tilde{w}
\end{aligned} \tag{13}$$

By neglecting products of disturbances, $\tilde{\omega}\tilde{i}_q$, $\tilde{\omega}\tilde{i}_d$ and $\tilde{i}_d\tilde{i}_q$, the PMSM state-space model is linearized and its representation in d-q coordinates is:

$$\begin{aligned}
\frac{d\tilde{i}_d}{dt} &= -\frac{R}{L_d}\tilde{i}_d + p\frac{L_q}{L_d}\Omega\tilde{i}_q + p\frac{L_q}{L_d}I_q\tilde{w} + \frac{1}{L_d}\tilde{v}_d \\
\frac{d\tilde{i}_q}{dt} &= -p\frac{L_d}{L_q}\Omega\tilde{i}_d - \frac{R}{L_q}\tilde{i}_q - p\frac{L_d}{L_q}I_d\tilde{w} - \frac{k_t}{L_q}\tilde{w} + \frac{1}{L_q}\tilde{v}_q \\
\frac{d\tilde{w}}{dt} &= \frac{3}{2J}(p(L_d - L_q)I_q\tilde{i}_d + (k_t + p(L_d - L_q)I_d)\tilde{i}_q) - \frac{k_{load}}{J}\tilde{w}
\end{aligned} \tag{14}$$

or, considering state-space variables as elements of vector $\tilde{x} = \begin{bmatrix}\tilde{i}_d & \tilde{i}_d & \tilde{w}\end{bmatrix}^t$ and input variables as elements of vector $\tilde{u} = \begin{bmatrix}\tilde{v}_d & \tilde{v}_q\end{bmatrix}^t$, it gives the vector representation of the small-signal state-space model of the PMSM drive:

$$\begin{aligned}
\dot{\tilde{x}} &= A\tilde{x} + B\tilde{u} \\
\tilde{y} &= C\tilde{x}
\end{aligned} \tag{15}$$

$$A = \begin{bmatrix} -\frac{R}{L_d} & p\frac{L_q}{L_d}W & p\frac{L_q}{L_d}I_q \\ -p\frac{L_d}{L_q}W & -\frac{R}{L_q} & -p\frac{L_d}{L_q}I_d \\ \frac{3}{2J}p(L_d - L_q)I_q & \frac{3}{2J}(k_t + p(L_d - L_q))I_d & -\frac{k_{load}}{J} \end{bmatrix} \qquad (16)$$

$$B = \begin{bmatrix} \frac{1}{L_d} & 0 \\ 0 & \frac{1}{L_q} \\ 0 & 0 \end{bmatrix} \qquad C = \begin{bmatrix} 1 & 0 & 0 \\ 0 & 1 & 0 \\ 0 & 0 & 1 \end{bmatrix}$$

By developing the characteristic polynomial, $P = det(sI - A)$, from Eq. (16), we can see that all poles depend on the operating point conditions. It emphasize the request that the control design must satisfy above described Bode criteria at all critical operating points.

The AC filter (Figure 5) d-q state-space linearized small-signal model, obtained following the same procedure, is:

$$\begin{aligned} \frac{d\tilde{i}_{Lfd}}{dt} &= p\Omega\tilde{i}_q + pI_{Lfq}\tilde{w} + \frac{1}{L_f}\tilde{v}_{cd} + \frac{1}{L_f}\tilde{v}_{din} \\ \frac{d\tilde{i}_{Lfq}}{dt} &= -p\Omega\tilde{i}_{Lfd} - pI_{Lfd}\tilde{w} - \frac{1}{L_f}\tilde{v}_{cq} + \frac{1}{L_f}\tilde{v}_{qin} \\ \frac{d\tilde{v}_{cd}}{dt} &= \frac{1}{C}\tilde{i}_{Lfd} + p\Omega\tilde{v}_{cq} + pV_{cq}\tilde{w} - \frac{1}{C}\tilde{i}_{outd} \\ \frac{d\tilde{v}_{cq}}{dt} &= \frac{1}{C}\tilde{i}_{Lfq} - p\Omega\tilde{v}_{cd} - pV_{cd}\tilde{w} - \frac{1}{C}\tilde{i}_{outd} \end{aligned} \qquad (17)$$

average model is represented in Figure 18.

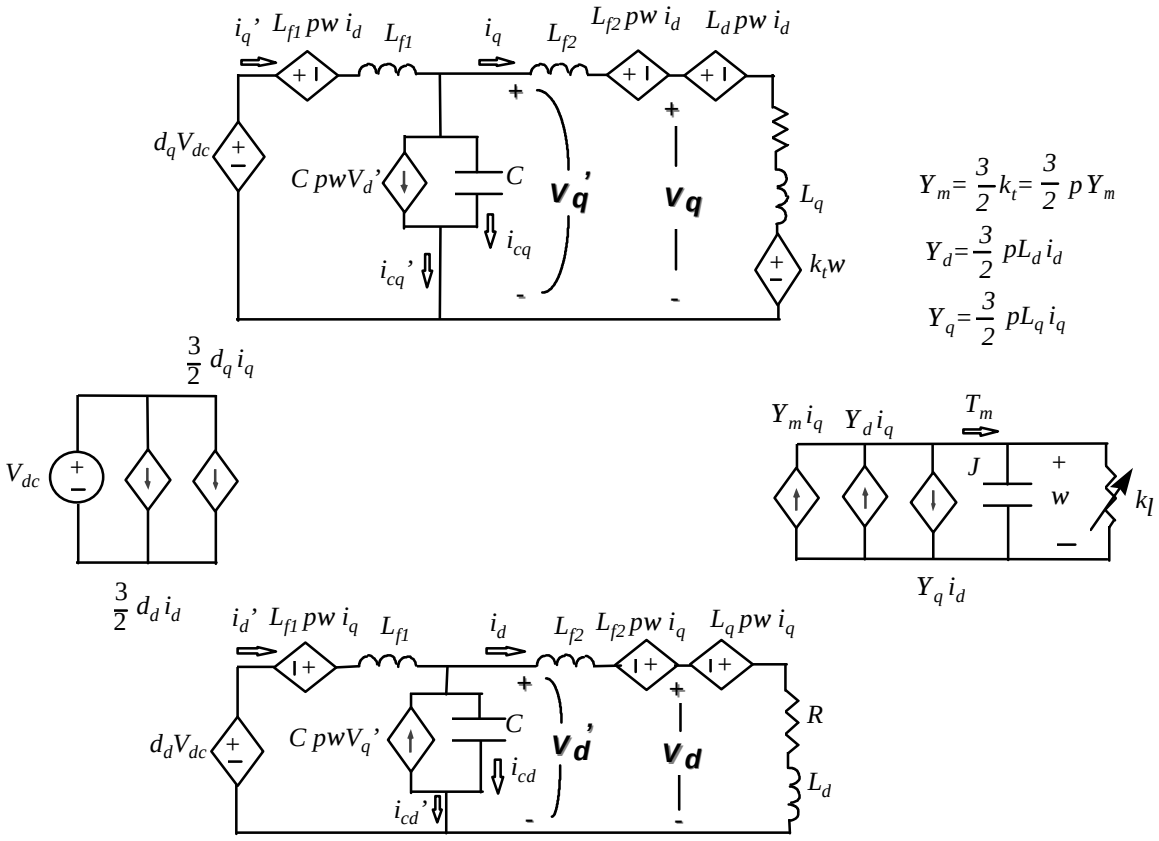

Figure 18. VSI fed PMSM drive (plant) d-q average model with a VSI output filter

Decoupling

In order to simplify the system by eliminating the coupling terms from the voltage Eq. (12), the so-called *decoupling control loop* coupling parts on the right-half side of $v_{d\quad q}$ state-space equations, signals of current loop PI controllers. In an ideal decoupling case, the decoupled motor model has the next derivation:

$$\left.\begin{aligned} v_d - pL_q w\, i_q &= Ri_d + L_d \frac{di_d}{dt} - pL_q w\, i_q \\ v_q + p_d L w\, i_d + k_t w &= Ri_q + L_q \frac{di_q}{dt} + pL_d w\, i_d + k_t w \end{aligned}\right\} \Rightarrow \begin{cases} v_d = Ri_d + L_d \dfrac{di_d}{dt} \\ v_q = Ri_q + L_q \dfrac{di_q}{dt} \end{cases} \tag{18}$$

The linearized small-signal state-space model, (18), can be represented in the vector form:

$$\begin{aligned} \dot{x} &= Ax + Bu \\ y &= Cx \end{aligned} \tag{19}$$

where

$$x = \begin{bmatrix} i_d \\ i_q \\ w \end{bmatrix}, \qquad u = \begin{bmatrix} v_d \\ v_q \end{bmatrix}, \qquad y = x \tag{20}$$

$$A = \begin{bmatrix} -\dfrac{R}{L_d} & 0 & 0 \\ 0 & -\dfrac{R}{L_q} & 0 \\ \dfrac{3}{2}\dfrac{p(L_d - L_q)}{J} I_q & \dfrac{3}{2}\dfrac{k_t}{J}\left(1 + \dfrac{p(L_d - L_q)}{k_t} I_d\right) & -\dfrac{1}{J} k_{load}{}^{*} \end{bmatrix}$$

$$B = \begin{bmatrix} \dfrac{1}{L_d} & 0 \\ 0 & \dfrac{1}{L_q} \\ 0 & 0 \end{bmatrix} \qquad C = \begin{bmatrix} 1 & 0 & 0 \\ 0 & 1 & 0 \\ 0 & 0 & 1 \end{bmatrix} \tag{21}$$

$$^{*}\textit{assumption}: \quad \Delta T_{load} = k_{load}(w - \Omega)$$

The poles of the system transfer functions are obtained from the system characteristic polynomial in s-domain:

$$-A = 0 \Rightarrow s_1 = -\frac{}{L_d}\,; s_2 = -\frac{}{L_q}\,; s_3 = -\frac{1}{}\,k_{load} \tag{22}$$

Because the design considers a two-loop cascade control, it is convenient to represent the decoupled PM motor model by an independent, i_d-current, transfer function:

$$G_d(s) = 1/\left(R + L_d\, s\right) \tag{23}$$

and a cascade of two transfer functions: i_q-current transfer function:

$$G_q(s) = 1/\left(R + L_q\, s\right) \tag{24}$$

and the electromechanical transfer function:

$$G_w(s) = 3k_t/(2(J + k_{load}\, s)) \tag{25}$$

which represent the equivalent DC motor with eliminated back-emf, Figure 19. The back-emf elimination is not necessary if $k_{load} > 0$ (without it, the well-known equivalent DC motor model is obtained in q-axis), but it simplifies the design because it establishes the same conditions (under an ideal decoupling) in both current loops, so their PI controllers can be equivalent (if $L_d = L_q$), or proportionally designed (if $L_d \neq L_q$), and, what is more important in this application, it assures current loop stability for every load condition (current loop becomes independent of load torque), i.e. it eliminates the influence of the load torque dynamics from the current control loops (see the following section).

Unfortunately, because of the current measurement filter, sampling and zero-order-hold delays in a digital controller, it is not possible to get an ideal decoupling. The filter influences the open-loop transfer function by uncoupled i_d and i_q current transfer functions. State space representation of a single-pole low-pass filter for current measurements in d-q coordinates is:

$$\begin{aligned} \frac{di_{dout}}{dt} &= w_f\,(i_{din} - i_{dout}) + pw\, i_{qout} \\ \frac{di_{qout}}{dt} &= w_f\,(i_{qin} - i_{qout}) - pw\, i_{dout} \end{aligned} \tag{26}$$

where

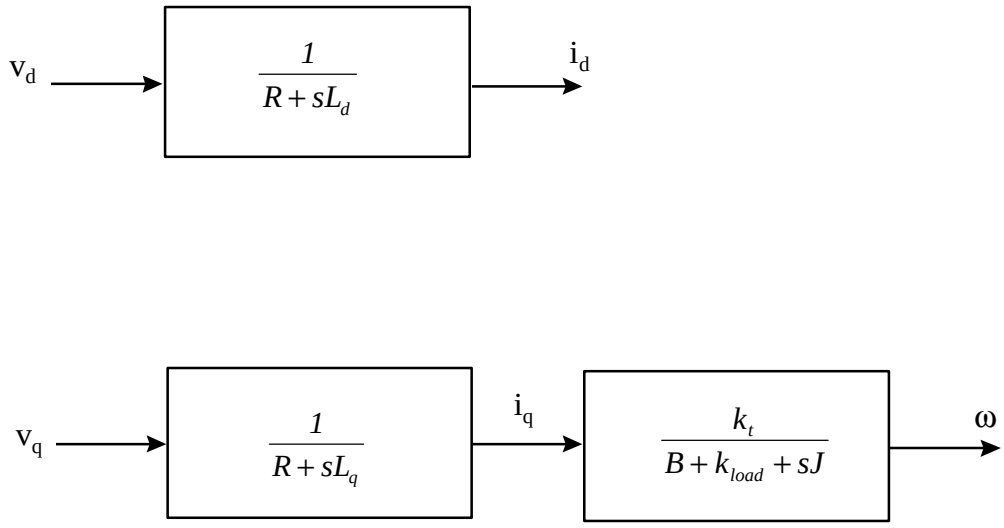

R - stator resistance
L_d - stator inductance in d-axis
L_q - stator inductance in q-axis

B - bearings
k_{load} - load torque slope
J - moment of inertia
k_t - motor torque constant

Figure 19. Decoupled PMSM drive block diagram

i_{dout}, i_{qout}: filter output current d-q comp. i_{din}, i_{qin}: filter input current d-q comp.

w_f: filter resonant frequency w: motor speed [rad/s]

p: number of the motor poles pairs

Hence, the current measurement filter produces non-linearity in the system. By choosing a high ω_f, i.e. above a half of the switching frequency, this negative effect on the loop-gain transfer function can be reduced, especially for a bandwidth much lower then ω_f (about five to ten times). The drawback is that switching and measurement noise will be less attenuated. The effect of sampling and zero-order-hold delay transfer functions on decoupling loops will be examined later in this chapter in a separate section.

A decoupling scheme for the whole drive system with the implemented AC filter (Figure 18) is shown in Figure 20. From the d-q system state-space model, it can be noticed that not only the motor d- and q-axis variables were coupled, but also all electrical variables of the three-phase system, related to energy storage elements (capacitors and inductors). The same conclusion made earlier for the current measurement filter can apply here. Consequently, only the largest filter LC components should be decoupled, so that a rough single-stage second-order approximation of the AC filter can serve for the decoupling circuit design. The small signal average model of the discussed drive system with the AC (EMI) filter, after the (ideal) decoupling without the back emf elimination, is shown in Figure 21. The modulation coefficient, m (for SVM $m = 1/\sqrt{3}$, for sinusoidal PWM $m = 1/2$), indicates a chosen modulation scheme [78].

3.2.1.3 Current Loop Controller Design

Two current control methods - with and without back emf elimination (equivalent DC motor control) through the decoupling - of the VSI fed PMSM drive system in an engine starter application will be discussed in this section. Although commonly used P regulators in current control loops can provide satisfactory results at lower speed (regarding the proximity of the line and switching frequency), in order to avoid problems related to sampling delay at higher motor speed, to eliminate steady-state error (although considerably small) and to increase the current loop bandwidth, thus speed-up the current response, the PI regulators are used in d and q current control loops.

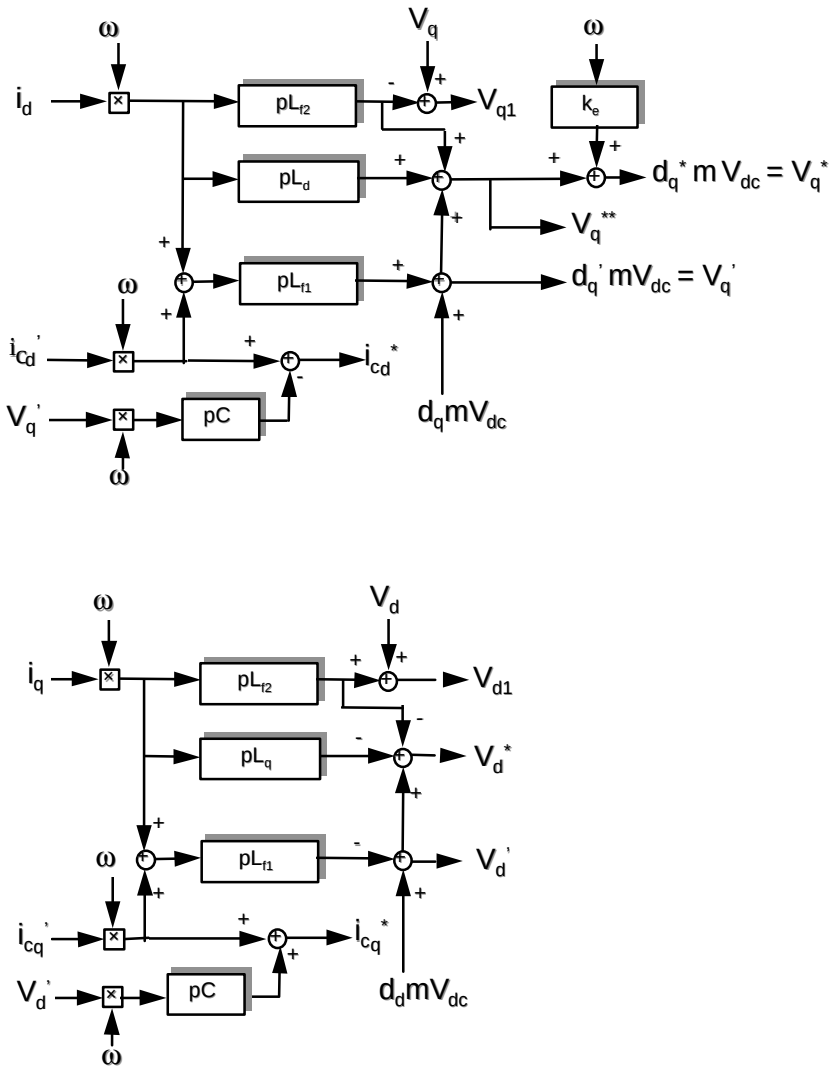

Figure 20. Decoupling scheme for the PMSM drive with a VSI output filter

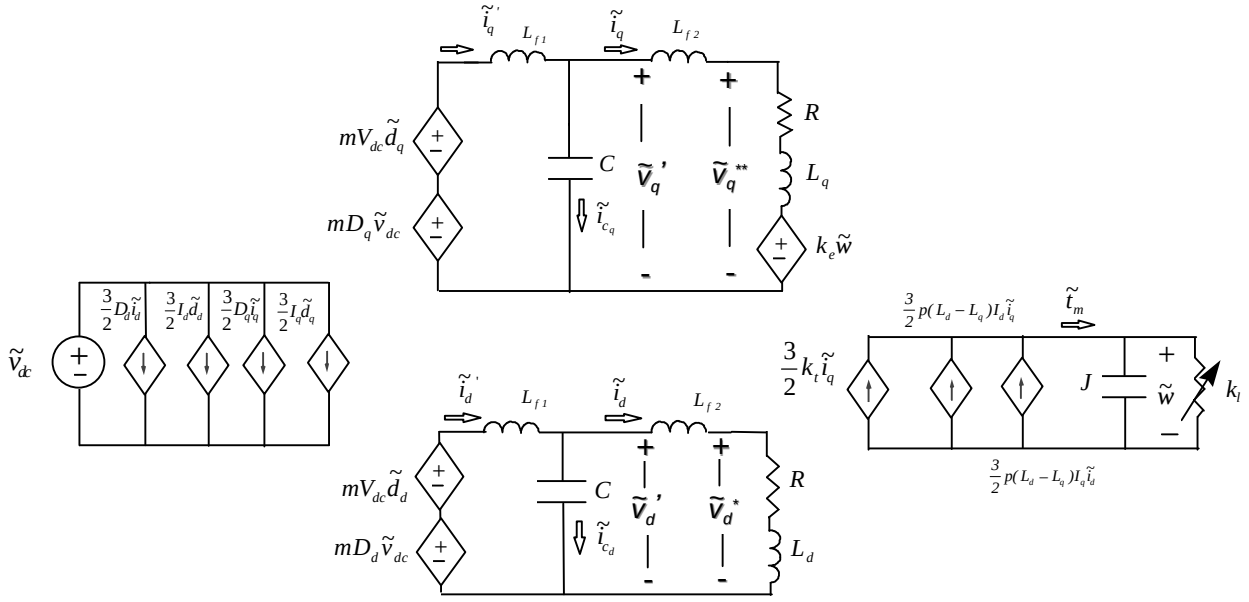

Figure 21. Dq small-signal average model of the linearized VSI-fed PMSM system with a three-phase EMI filter and without back emf elimination

Current loop-gain transfer function of the decoupled motor drive with back-emf elimination with used PI compensator in the current loops is

$$T(s) = K_{im} \frac{K_p s + K_i}{s} \frac{mV_{dc}}{(R + Ls)} \tag{27}$$

where K_p and K_i are PI compensator proportional and integral gains, respectively, L is the inductance in a considered loop, and K_{im} is a current measurement scaling factor due to the signal normalization [18, 52, 57]. The pole of the current measurement filter is considered high enough to be neglected, for the sake of simplicity. In an ideal decoupling, the choice of

$$\frac{K_p}{K_i} = \frac{L}{R} \tag{28}$$

gives a phase margin of 90^o more than what is needed, and, in order to provide a larger bandwidth, it can be set from Eq. (27) after some elementary trigonometric calculation that:

$$\arctan(\frac{K_p w_c}{K_i}) - \arctan(\frac{L w_c}{R}) - 90^o \geq -180^o + pm \Rightarrow \frac{K_p}{K_i} > \frac{L}{R} \tag{29}$$

From the equation for the magnitude at w_c:

$$\left|T(s)\right| = mV_{dc} K_{im} \frac{1}{w_c} \sqrt{\frac{K_i^2 + (K_p w_c)^2}{R^2 + (L w_c)^2}} = 1 \tag{30}$$

and Eq. (29) we can calculate PI gains K_p and K_i for a desired bandwidth, ω_c, and phase margin, pm. Eq.s (29) and (30) should be used for the design check-out, i.e. for the calculation of the gain at the phase of -180^o and its comparison with the assigned gain margin of 6 dB.

Finally, the expression for the closed loop transfer function is:

$$\begin{aligned} T_{cl}(s) &= \frac{T(s)}{1 + T(s))} = \frac{mV_{dc} K_{im} (K_p s + K_i)}{s(R + Ls) + mV_{dc} K_{im} (K_p s + K_i)} = \\ &= \frac{\frac{K_p}{K_i} s + 1}{\frac{L}{mV_{dc} K_{im} K_i} s^2 + \left[\frac{R}{mV_{dc} K_{im} K_i} + \frac{K_p}{K_i}\right] s + 1} \end{aligned} \tag{31}$$

When a three-phase AC filter, Figure 21, is included in the PMSM drive system, the current control-to-output transfer functions of the decoupled system, depending on which of two control methods is chosen, are:

a) decoupling with back emf elimination:

$$\frac{\tilde{i}_q}{\tilde{d}_q} = mV_{dc}\,\frac{1}{CL_{f1}(L_{f2}+L_q)s^3 + CL_{f1}Rs^2 + (L_{f1}+L_{f2})s + L_q s + R} \tag{32}$$

Usually $L_{f1}<<L_{f2}<L_q$ and $w_c << 1/\sqrt{CL_{f1}}$, so that in the vicinity of the cross-over frequency, Eq. (32) can be approximated as:

$$\frac{\tilde{i}_q}{\tilde{d}_q} = mV_{dc}\,\frac{1}{(L_{f1}+L_{f2}+L_q)s + R} \tag{33}$$

b) decoupling without back emf elimination:

$$\frac{\tilde{i}_q}{\tilde{d}_q} = \frac{mV_{dc}\left(Js+k_{load}\right)}{\left(Js+k_{load}\right)\left[CL_{f1}(L_{f2}+L_q)s^3 + CL_{f1}Rs^2 + (L_{f1}+L_{f2})s + L_q s + R\right] + \frac{3}{2}k_t k_e (L_{f1}s+1)} \tag{34}$$

In the vicinity of the cross-over frequency the Eq. (34) can be approximated as:

$$\begin{aligned}\frac{\tilde{i}_q}{\tilde{d}_q} &= mV_{dc}\,\frac{Js+k_{load}}{\left(Js+k_{load}\right)\left(\left(L_{f1}+L_{f2}+L_q\right)s+R\right)+\frac{3}{2}k_t k_e} \\ &= mV_{dc}\,\frac{Js+k_{load}}{JL_{eq}s^2 + \left(RJ + L_{eq}k_{load}\right)s + k_{load}R + \frac{3}{2}k_t k_e}\end{aligned} \tag{35}$$

where $L_{eq}=L_{f1}+L_{f2}+L_q$. The torque constant k_t, and back emf constant k_e, are equal if the motor is not saturated. The similarity between Eq.s (27) and (33) is obvious, so that the PI compensator design procedure is the same as described through the Eq.s (28) to (31).

As the back emf is proportional to speed, it is also influenced by the load torque profile. Consequently, if the back emf is not eliminated from i_q current loop through the decoupling, the current loop will also be affected by the load torque profile. This influence can be seen in the simplified i_q control-to-output transfer function Eq. (35). It should be noticed that the condition $k_{load} < 0$ is a destabilizing factor, depending also on the system parameters R, J and L_{eq}. The comparison between two observed current control methods - with and without back emf elimination - can be summarized by the following characterization:

1. Control with back emf elimination characteristics:

- current loops are independent of each other and of the mechanical circuit;

- load torque profile cannot destabilize current loops;

- mechanical pole appears unchanged in the speed loop TF; and

- speed loop can be stabilized by matching the reference motor torque slope with the load torque slope, what will be shown later in the speed control design.

2. Control without back emf elimination (equivalent DC motor) characteristics:

- i_d current, if not equal to zero, influences i_q current loop through the back emf, thus the system is not completely decoupled;

- i_q current loop also depends on the mechanical circuit, i.e. the load torque influences the i_q current loop and can destabilize it;

- mechanical pole is slightly moved toward the left half plane in the speed control-to-output transfer function, what allows a higher bandwidth.

To improve the current controller characteristics, it is possible to design an adaptive PI controller [53, 79, 80], i.e. to optimize the drive performances at every operating point. It should have adaptive gains according to the load torque profile approximation in real-time, which will be discussed in a later section. A detailed non-linear design of such a controller could cover another master's thesis, and thus it is beyond the scope of this work.

3.2.1.4 Sampling Delay Considerations

A sampling delay transfer function can be approximated by Pade's formula, obtained from the McLorain's polynomial derivative of the sampling delay transfer function [11]:

$$G_{sd}(s) = e^{-sT_d} \approx \frac{\frac{1}{12}s^2T_d^{\,2} - 0.5sT_d + 1}{\frac{1}{12}s^2T_d^{\,2} + 0.5sT_d + 1} \tag{36}$$

where T_d is the sampling delay time constant. The zero-order-hold delay is approximated by:

$$G_{zoh}(s) = \frac{sT_z}{1 - e^{-sT_z}} \approx \frac{1}{\frac{1}{12}s^2T_z^{\,2} + 0.5sT_z + 1} \tag{37}$$

where T_z is the zero-order-hold delay time constant. The sampling delay time constant, T_d, and the zero-order-hold delay time constant, T_z, cannot be smaller than one switching period and in this application they are both approximated to be 1.5 times larger than the switching period.

Defining the sampling delay and zero-order-hold delay time constants determines the zeros and poles of the approximated delay transfer functions, and their corner frequencies can be calculated from Eq.s (36) and (37):

$$\left.\begin{aligned} s_z &= \frac{3}{T_d} \qquad for\ zeros; \quad s_p = -\frac{3}{T_d} \quad for\ poles \\ T_d &= 1.5\,T_s \end{aligned}\right\} \Rightarrow w_z = w_p = 2w_s \tag{38}$$

Because of their high corner frequencies, it could be expected that the influence of sampling and zero-order-hold delays on the system transfer function is small under low frequency. However, because of the high phase drop in the current loop-gain transfer function (about 360^o at the frequency of zeros and poles of the sampling delay approximate model, i.e. at a double switching frequency in our case), the sampling delay has a significant influence on the magnitude and phase of the loop-gain transfer function (see Figure 12 in Chapter 2). If the cross-over frequency is chosen to be around one tenth of the switching frequency, a rough approximation of the phase drop due to sampling delay is 45^o. So, by choosing PI gain ratio from Equation (34) we are getting a phase margin of 45^o instead of 90^o, as in the ideal case.

Knowing the conditions above mentioned, after the design of the current controller parameters, we can plot Bode plots for current loop-gain and closed loop transfer functions at different operating points and choose the critical ones. The critical operating points are those where the acceleration of the motor increases. In other words, the critical operating points are where the difference between motor and load torque resistances (slopes) rises significantly, because it defines the moving of the electromechanical pole $((k_{load}-k_t)/J)$ toward the unstable right half-plane of the root-locus diagram. Because of an non-ideal decoupling (undecoupled measurement filter, delays, decoupling transients, and parameter mismatching), the results can be different than expected at higher speed, where the influence of the digital delay on the phase of the loop-gain transfer function can be significant. The gains of the PI controllers in current loops should be adjusted to achieve the most satisfying results at all critical operating points.

By implementing Eq.s (37) and (38) in the control system described by (27), the closed current loop transfer function of the current regulated motor drive, with the sampling delay included, is

$$T_{cl}(s) = \frac{T(s)G_{sd}(s)}{1 + T(s)G_{sd}(s)} G_{zoh}(s) = \frac{1}{\dfrac{s(R + Ls)}{mV_{dc}K_{im}(K_p s + K_i)G_{sd}(s)} + 1} G_{zoh}(s) \tag{39}$$

In the case of a desired complete decoupling, the sampling delay can produce the instability of the current loops. To prove it, let's define voltage v_c as a coupling term in the motor large signal model, Eq. (12), shown in Figure 4, and v_{cfb} decoupling signal from the decoupling circuit, Eq. (18). The idea of canceling the coupling terms is to produce two reduced order decoupled systems in the d and q axis. But, the current and speed feedback signals are sampled, thus delayed, and a general case decoupling function becomes

$$DTF(s) = v_c - v_{cfb} = \left[1 - G_d(s)\right]v_c = v_c\left(1 - e^{-sT_d}\right) \approx \frac{-T_d s}{1 + \frac{1}{2}T_d s + \frac{1}{12}T_d^2 s^2} v_c \tag{40}$$

The unstabilizing factor is the zero of the decoupling transfer function, placed in the origin with the additional 180^o phase shift. This problem is clearly the result of an overcompensation. To avoid such a problem, a scaling factor, denoted as α, is added as a gain in the decoupling circuit. Now, the decoupling equation becomes

$$\begin{aligned} DTF(s) = v_c - v_{cfb} &= \left[1 - a\, G_d(s)\right]v_c = \left(1 - a\, e^{-sT_d}\right)v_c \\ &\approx \frac{1 - a - (1 + a)\frac{1}{2}T_d s + (1 - a)\frac{1}{12}T_d^2 s^2}{1 + \frac{1}{2}T_d s + \frac{1}{12}T_d^2 s^2} v_c \end{aligned} \tag{41}$$

The scaling factor α should have a value $0 < \alpha < 1$ to avoid the overcompensation. A general rule should be that smaller sampling delay allows α to be closer to unity.

The sampling delay can be implemented in a reference current signal because the current reference doesn't change as quickly, compared to the sampling delay time constant. From the elementary graph theory, it is implied that the sampling delay transfer function can be moved to the output of the current compensator. Then, the current compensator transfer function, considering the sampling delay transfer function, becomes:

$$H_j(s) = \frac{K_{pj} s + K_{ij}}{s} G_{sd}(s) \tag{42}$$

Index *j* denotes the d- or q-axis current loop. Current loop-gain transfer function with back-emf elimination decoupling in the vicinity of the crossover frequency becomes

$$l_i(s) = mV_{dc}\frac{1}{(L_{f1}+L_{f2}+L_i)s+R}H_i(s)G_{sd}(s) \tag{43}$$

Index *i* denotes the d- or q-axis current loop.

The current loop-gain transfer function in the q-axis with the decoupling without back emf elimination, in the vicinity of the crossover frequency, has the expression

$$l_q(s) = mV_{dc}\frac{Js+k_{load}}{JL_{eq}s^2+\left(RJ+L_{eq}k_{load}\right)s+k_lR+\frac{3}{2}k_tk_e}H_q(s)G_{sd}(s) \tag{44}$$

The current loop-gain transfer function in the d-axis is the same for both methods, Eq. (43).

The current controller design procedure remains the same, but with a caution about the phase margin reduction due to the sampling delay.

3.2.1.5 Speed Loop Controller Design

Usually, design of the speed loop controller is based on the fact that the pole of the electromechanical transfer function, Eq. (25), $s_w = k_{load}/J$, is at a much lower frequency than the crossover frequency of the closed current loop transfer function, $T_{cl}(s)$ [52]. A common torque control method in PMSM motor drives is to keep $i_d = 0$ (although with interior permanent magnet (IPM) motors this is not the optimal approach because of the unused reluctant torque component [41, 42, 70]), so it will be assumed that it is applied in this case, for the sake of simplicity. Under these assumptions, a speed control-to-output transfer function (TF) with closed current loop (reference-i_q-current-to-speed TF) has the next form:

$$G_{i_{qref}-w}(s) = \frac{3k_t}{2}\frac{1}{k_{load}+Js} \tag{45}$$

Using the PI compensator and adding the speed-to-control signal conversion factor, $K_{\omega m}$, in both the speed feedback and reference signal paths, the speed loop-gain TF becomes

$$T_w = K_{wm}\frac{K_{pw}s+K_{iw}}{s}G_{i_{qref}-w}(s) = K_{wm}\frac{3k_t}{2}\frac{K_{pw}s+K_{iw}}{s(k_{load}+Js)} \tag{46}$$

In a stable system ($k_{load}>0$), with known k_{load}, it is reasonable to put the compensator zero in the vicinity of the pole of the speed open loop TF, producing a relatively high bandwidth. In order to optimize the design, the compensator zero can be placed above the pole frequency, as

long as it assures a sufficiently large phase margin whenever the gain is above -6 dB (k_{load} is not the same in all operating points!), as was shown previously in the current controller design.

Closed speed loop TF is now trivial:

$$T_{wcl} = \frac{T_w}{1+T_w} = \frac{1}{\frac{s}{K_{w\,m}\frac{3k_t}{2}\frac{K_{iw}}{k_{load}}}+1} \tag{47}$$

But, when the speed open loop TF pole is unstable, i.e. $k_{load} < 0$, the compensator zero can compensate the pole regarding the gain characteristics (Bode diagram), but their phases add to each other and produce a phase shift of 180 degrees. Thus, without the decrease of the reference torque by a torque with a slope higher than $|k_{load}|$, the speed loop-gain TF should be considered unstable. Passive compensator effects are most considerable at low speed, where $k_{load} \geq 0$, at the final speed, where a reference speed is reached, and in failure modes of operation (e.g., sudden load disconnection), where it prevents the motor overrun. Otherwise, the system mainly operates with the saturated speed compensator output, i.e. with an open speed loop.

The other commonly used method for the speed controller design is the symmetrical optimum, a well-known method in industry, widely used for DC motor drive speed control [38, 57, 62]. It is usually applied when the poles of the electromechanical and current closed loop transfer functions are insufficiently separated, or when the speed measurement filter has a low pole which cannot be neglected, i.e. when the closed current loop (or filter) TF should be approximated as the first order TF, i.e. from Eq.s (28) and (31):

$$T_{cl}(s) \approx \frac{1}{\frac{R}{mV_{dc}K_{im}K_i}s+1} \tag{48}$$

or if it is chosen $K_i=0$ (P current regulator):

$$T_{cl}(s) = \left(\frac{1}{\frac{R}{mV_{dc}K_{im}K_p}+1}\right)\left(\frac{1}{1+\frac{L}{R+mV_{dc}K_{im}K_p}s}\right) \tag{49}$$

Now, the speed loop-gain transfer function has a form:

$$T_w'(s) = K_{wm}\frac{K_{pw}s + K_{iw}}{s(k_{load} + Js)}T_{cl}(s) = K_w\frac{\frac{s}{s_1}+1}{s(\frac{s}{s_2}+1)(\frac{s}{s_3}+1)} \quad (50)$$

where $s_1 = \frac{K_{iw}}{K_{pw}}$, $s_2 = s_w = \frac{k_{load}}{J}$, s_3 is the pole of $T_{cl}(s)$ transfer function, K_ω is a speed error ($\lim_{s\to 0}(sT_w'(s))$) of the speed loop-gain TF $T_\omega'(s)$, and $K_{\omega m}$ is the speed measurement scaling factor. The closed speed loop TF is now

$$T_{w\,cl\_sym.opt.} = \frac{T_w'}{1+T_w'} = \frac{\frac{s}{s_1}+1}{\frac{s(\frac{s}{s_2}+1)(\frac{s}{s_3}+1)}{K_w} + \frac{s}{s_1}+1} \quad (51)$$

From the calculations of the maximum gain of the closed speed loop TF, the two compensator gains are obtained as

$$K_{iw} = \frac{k_{load}}{\frac{3k_t}{2}K_{wm}}\frac{(s_2+s_3)^3}{8s_1s_2} \quad and \quad K_{pw} = 4K_{iw}\frac{s_2^2+s_3^2}{(s_2+s_3)^3} \quad (52)$$

Again, the method is not reliable for $k_{load} < 0$. The conclusion related to the former design holds for this design too.

A speed controller design for the maximum torque operating region holds also inside the flux-weakening region, because during the flux-weakening the motor torque decreases, so does the acceleration, and the system behavior is supposed to be even more stable. A more detailed discussion of the flux-weakening techniques is given in Section 3.2.3.

3.2.1.6 Speed Loop Stabilization

It is evident from the previous section, that in the case of the active load produced during an engine acceleration, Figure 14, the speed loop cannot be stabilized (at least the local instability will remain) by applying only a two stage cascade static controller.

There are several methods proposed in the literature for the speed loop design [21, 39, 45, 52]. Most of them are based on the observer predictive control designs, which are very sensitive to the system parameter mismatching and relatively complicated for realization. Here the

proposed methods are based on the extraction of the information about the load torque slope, k_{load}, Eq. (12), from the measurements of the motor terminal currents and voltages. The same information could also serve in the $k_{load} > 0$ case to improve the controller speed performance at different operating points, especially if k_{load} changes dynamically with speed, which is the case with the torque profile from Figure 14. In order to derive information about the load torque slope, the load torque profile (including friction) is approximated as a sum of incrementally piece-wise linear parts, Figure 14. As long as the motor electromechanical time constant is much bigger than a switching cycle of the VSI, the load torque incremental periods are also much longer than the VSI switching cycle. It is assumed that during these incremental periods the load torque slope can be approximated using linear interpolation. A result can be either kept in memory until the next significant change of the load torque slope, or continually estimated through the current and voltage sensing. Now, from the motor state-space system of equations, Eq. (12), the expression for the k_{load}, Eq. (56), can be derived by deriving the speed equation either from the d-axis or from q-axis voltage Eq.s (53) and (54), respectively,

$$w = \frac{-v_d + Ri_d + L_d \frac{di_d}{dt}}{pL_q i_q} \tag{53}$$

$$w = \frac{v_q - Ri_q - L_q \frac{di_q}{dt}}{pL_d i_d + k_t} \tag{54}$$

Calculating the speed derivative from Eq. (53) and substituting the speed and its derivative to the motor electromechanical (torque) Eq. (55),

$$k_{loadi} = \frac{T_m - T_{loadi} - J\frac{dw}{dt}}{w - W_i} \tag{55}$$

the load torque slope is calculated from Eq. (56):

$$k_{loadi} = \frac{T_m - T_{loadi} - \frac{J}{pL_q i_q}\left[-\frac{dv_d}{dt} + R\frac{di_d}{dt} + L_d\frac{d^2 i_d}{dt^2} - (-v_d + Ri_d + L_d\frac{di_d}{dt})\frac{1}{i_q}\frac{di_q}{dt}\right]}{w - W_i} \tag{56}$$

where $T_{loadi} = T_{load0} + \sum_i k_{loadi}(W_{i+1} - W_i)$ is the load torque at the beginning of the i-th incremental period, $T_m = \frac{3}{2}(k_t i_q + p(L_d - L_q) i_q i_d)$ is the motor torque, either measured directly, or evaluated through the current measurements, and Ω_i is the speed where load torque slope significantly changes i-th time.

In order to avoid problems related to differentiation in control loops (e.g. increasing the noise signal effect), a VSI output filter can be used, $L_{f1}C$ (a simple LC structure is used here for the sake of simplicity), in series with an external inductance, L_{f2}, on the motor terminals, to extract the state-space variables related to voltage and current derivatives. A complete unregulated PMSM drive system large-signal d-q model is shown in Figure 18. The decoupling scheme for such a system is given in Figure 20, while a small-signal model of the decoupled system is given in Figure 21. Voltage signals v_q, v_{q1}, v_q^*, v_q^{**}, v_q', v_d, v_{d1}, v_d^*, v_d' and current signals i_{cd}^* and i_{cq}^* are used for the load torque slope evaluation to substitute current and voltage derivatives in Eq. (56):

$$\begin{aligned} \frac{di_d}{dt} &= \frac{1}{L_f}(v_d' - v_{d1}); \quad \frac{dv_d'}{dt} = \frac{1}{C} i_{cd}^* \\ \frac{di_q}{dt} &= \frac{1}{L_f}(v_q' - v_{q1}); \quad \frac{dv_q'}{dt} = \frac{1}{C} i_{cq}^* \end{aligned} \tag{57}$$

which results in the next expression:

$$\begin{aligned} k_{loadi} = {} & \frac{T_m - T_{loadi} - \frac{J}{pL_q i_q}\left[-\frac{dv_d}{dt} + \frac{R}{L_{f2}}(v_d' - v_{d1}) + \frac{L_d}{L_{f2}}\left(\frac{1}{C} i_{cd}^* - \frac{d v_{d1}}{dt}\right)\right]}{\frac{-v_d + R i_d + \frac{L_d}{L_{f2}}(v_d' - v_{d1})}{pL_q i_q} - W_i} + \\ & + \frac{\frac{J}{pL_q i_q}\left[-v_d + R i_d + \frac{L_d}{L_{f2}}(v_d' - v_{d1})\right]\frac{1}{L_{f2} i_q}(v_q' - v_{q1})}{\frac{-v_d + R i_d + \frac{L_d}{L_{f2}}(v_d' - v_{d1})}{pL_q i_q} - W_i} \end{aligned} \tag{58}$$

By substituting the torque equation from Eq. (12) into Eq. (58) and after some reshaping, we get:

$$k_{loadi} = \frac{pL_q i_q}{v_i}\left(\frac{3}{2}\left(k_t i_q + p(L_d - L_q) i_d i_q\right) - T_{loadi}\right) -$$

$$\frac{J}{v_i}\left[-\frac{dv_d}{dt} + \frac{R}{L_{f2}}(v_d^{'} - v_{d1}) + \frac{L_d}{L_{f2}}\left(\frac{1}{C} i_{cd}^{*} - \frac{d\,v_{d1}}{dt}\right) - \frac{v_i + pW_i L_q i_q}{L_{f2}\, i_q}(v_q^{'} - v_{q1})\right],$$

$$v_i = -v_d + R i_d + \frac{L_d}{L_{f2}}(v_d^{'} - v_{d1}) - pW_i L_q i_q \tag{59}$$

A closer look at Eq. (59) reveals that the only new terms comparing with the decoupling Eq. (18), are the d-q components of decoupled filter input and output (motor terminal) voltages and their derivatives, and decoupled filter capacitance current. Troublesome differentiation of current signals from Eq. (56) is replaced with the only first order differentiation of two digitally filtered voltage signals in Eq. (59). Assuming that the coupling effect of the filter inductance L_{f1} can be neglected because of relatively small inductance L_{f1} in comparison with the relevant inductances of the drive system, L_d, L_q and L_{f2}, the first derivatives of voltages v_d' and v_q' can be approximated with the derivatives of the corresponding PI controller outputs, $d_d^{'} \approx d_d$ and $d_q^{'} \approx d_q$, in the average sense (after passing the low pass filter), multiplied by a scaled DC link voltage (maximum phase to neutral voltage). As all the voltage variables involved in the k_{load} calculations are measured after passing through the low pass filter ($L_{f1}C$), there are no high order harmonics in their spectra, so their measurements and their first derivatives should not produce any problematic noise which could affect the accuracy of the k_{load} estimation. In this application, it no fast changes of the load torque are expected (it is much more than ten times slower than the VSI switching), so the estimated average value of the load torque slope can be assumed as an appropriate estimation. The weak points of this method are problematic measurements of the motor terminal voltages and filter capacitor currents due to a high level of noise in those signals. However, the low load dynamics allow good filtering of these signals and their sensing is already known in industrial and academic practice, mainly in sensorless control applications [21, 39, 45].

A modified design of the speed loop will be based on the assumption that the current control is done with back emf elimination and that the mechanical pole is much lower than the pole of the closed current loop pole, so the closed current loop transfer function can be approximated as a unity gain. The design for $k_{load} > 0$ (so-called positive load resistance) follows

the previously explained procedure with a note that, due to the mechanical pole estimation, the compensator gains can be adapted to optimize the system performances at different operating points. However, a negative load resistance, $k_{load} < 0$, produces an unstable pole in the speed control-to-output transfer function, Eq.s (22) and (25):

$$G_w(s) = \frac{3}{2} k_t \frac{1}{k_{load} + Js} \Rightarrow \textit{right half plane pole for } k_{load} < 0 \tag{60}$$

In order to stabilize the speed loop, a term proportional to the estimated load torque change is added to the motor torque reference, Figure 22, and such a modified motor torque profile determines the current reference, (61):

$$\begin{aligned} J\frac{d\tilde{w}}{dt} &= \tilde{t}_m + s k_{load}\tilde{w} - k_{load}\tilde{w} \\ G_w(s) &= \frac{\frac{3}{2}k_t}{(1-s)k_{load} + Js} \Rightarrow \textit{stabilized pole for } k_{load} < 0 \end{aligned} \tag{61}$$

A scaling factor, σ, can be adjusted to provide a desired mechanical pole, but should be larger than one in order to establish a safety margin in the motor torque profile, but also kept to a minimum. In the case when $k_{load} > 0$, σ should be kept equal to zero for the maximum torque profile. Further speed controller design procedure remains the same as explained earlier. Simulation results of a PMSM drive system small-signal analysis are discussed in Chapter 4.

Finally, it should be noted that there are a lot of possibilities for designing a non-linear and/or adaptive control with variable compensator gains, based on the load torque slope estimation, but it will be left for the future work.

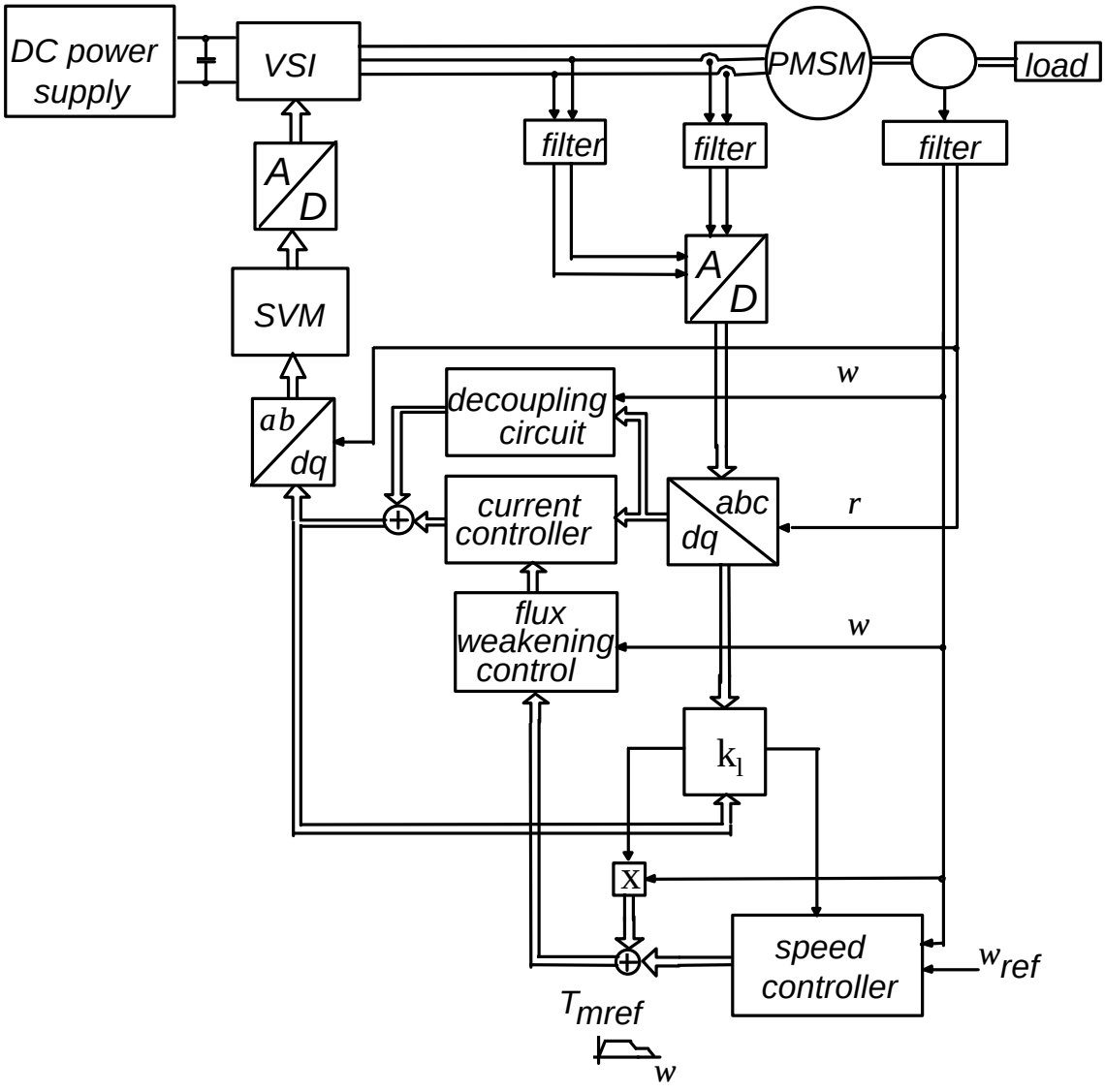

Figure 22. Reference motor torque and speed controller adjustments to active load for the speed loop stabilization